Supplement of Atmos. Chem. Phys., 22, 15263–15285, 2022
https://doi.org/10.5194/acp-22-15263-2022-supplement

Atmospheric Chemistry and Physics
Open Access
EGU

Supplement of

Atmospheric particle abundance and sea salt aerosol observations in the springtime Arctic: a focus on blowing snow and leads

Qianjie Chen et al.

Correspondence to: Kerri A. Pratt (prattka@umich.edu)

Supplementary Information

Text S1 provides supplementary results and discussion of the chemical composition of atmospheric particles during moderate wind speed periods, during observed and falsely predicted blowing snow periods, and regarding sea salt aerosol sources during observed blowing snow. Text S2 describes the organic+sulfate aerosol particles identified by CCSEM-EDX. The NOAA Barrow Observatory submicron and supermicron particle [NH_4^+], [NO_3^-], [Br^-], methanesulfonate ([MSA^-]), and oxalate mass concentration data are shown in Table S1 for the time periods of interest for reference. Submicron and supermicron particle [Na^+], [Cl^-], [SO_4^{2-}], [Ca^{2+}], [Mg^{2+}], and [K^+] mass concentration data are shown in Table S2. Table S3 shows the [Cl^-]/[Na^+], [SO_4^{2-}]/[Na^+], [Ca^{2+}][Na^+], [Mg^{2+}]/[Na^+], and [K^+]/[Na^+] molar ratios for submicron and supermicron particles, local tundra surface snowpack, and previous measurements of sea ice surface snowpack, blowing snow, frost flowers, and seawater. Table S4 shows the Na^+, K^+, Ca^{2+}, Mg^{2+}, Cl^-, NO_3^-, Br^-, and SO_4^{2-} concentrations for local tundra surface snowpack samples. Table S5 shows the particle number concentrations in different size bins and wind categories observed during the study. Figure S1 shows the time-resolved size distributions of ambient particles measured by an optical particle sizer (OPS) and a scanning mobility particle sizer (SMPS). The comparison of total particle number concentrations measured by SMPS and CPC is shown in Figure S2. The size-resolved numbers of particles measured by CCSEM-EDX for the four samples collected during this study are shown in Figure S3. The representative SEM images and EDX spectra of the main particle types observed are shown in Figure S4. Digital color histograms of the EDX spectra of individual 0.4-2.8 μm da fresh sea spray aerosol particles are shown in Figure S5. The elevation map of our field site and its surroundings is shown in Figure S6. The meteorological conditions at our field site, Wiley Post-Will Rogers Memorial Airport, and the Department of Energy Atmospheric Radiation Measurement (ARM) Observatory are shown in Figure S7.

S1. Additional results and discussion of the chemical composition of atmospheric particles

S1.1 Moderate wind speed periods

In this study, individual dust (mainly aluminum and silicon-containing, with some calcium), soot, and potassium+sulfur (presumably in the form of sulfate) aerosol particles comprised 0-31%, 0-15%, and 0-6%, by number, respectively, across the 0.09-0.9 μm d_{pa} range (d_a 0.07-0.4 μm impactor stage) on April 15-16 (Fig. 6a). During April 15-16, submicron particle non-sea-salt calcium, magnesium, and potassium mole fractions ($f_{nssCa^{2+}}$, $f_{nssMg^{2+}}$, and f_{nssK^+}) were calculated to be 77%,

25%, and 78%, respectively, consistent with the observed submicron dust and potassium+sulfur aerosol particles. Similar to the low wind periods, the submicron particle $[K^+]/[Na^+]$ (average 0.09±0.05 mol mol^{-1}) and $[Ca^{2+}]/[Na^+]$ (average 0.08±0.03 mol mol^{-1}) were higher than those of seawater (both 0.02 mol mol^{-1}; Millero et al., 2008) during moderate wind periods (Fig. 5), consistent with contributions from long-range transported aerosols during springtime Arctic haze in Utqiaġvik (Quinn et al., 2002; 2007).

Note that Mg was also enriched (Mg/Na = 0.6±0.3 during April 15-16; 0.5±0.2 during April 16) in the 0.07-0.4 μm d_a individual sea spray aerosol particles (Table 3), compared to seawater (0.11; Millero et al., 2008). This divalent cation binds with organic matter (exopolymeric substances; Krembs et al., 2002) within the sea surface microlayer, resulting in magnesium-enriched organic coatings on the sea salt aerosol (Jayarathne et al., 2016; Bertram et al., 2018; Kirpes et al., 2019).

Individual potassium chloride and mineral dust particles accounted for 67±8%, and 3±2%, on average by number, respectively, of the particles, respectively, collected during April 15-16 and April 16 on the 0.4-2.8 μm d_a impactor stage. For the April 28 – May 4 supermicron particle sample, the non-sea-salt mole fractions of calcium ($f_{\mathrm{nssCa^{2+}}}$, *SE*1), magnesium ($f_{\mathrm{nssMg^{2+}}}$, *SE*2), and potassium ($f_{\mathrm{nssK^{+}}}$, *SE*3) were 88%, 51%, and 71%, respectively, consistent with the observed individual potassium chloride and mineral dust particles. SE1-SE3 were previously defined by Quinn et al. (2002).

$$f_{\mathrm{nssCa^{2+}}} = \frac{\mathrm{Total\ Ca^{2+}} - 0.02\mathrm{Na^{+}}}{\mathrm{Total\ Ca^{2+}}} \qquad (SE1)$$

$$f_{\mathrm{nssMg^{2+}}} = \frac{\mathrm{Total\ Mg^{2+}} - 0.11\mathrm{Na^{+}}}{\mathrm{Total\ Mg^{2+}}} \qquad (SE2)$$

$$f_{\mathrm{nssK^{+}}} = \frac{\mathrm{Total\ K^{+}} - 0.02\mathrm{Na^{+}}}{\mathrm{Total\ K^{+}}} \qquad (SE3)$$

For comparison, during April 28 – May 4, submicron particle $f_{\mathrm{nssCa^{2+}}}$, $f_{\mathrm{nssMg^{2+}}}$, and $f_{\mathrm{nssK^{+}}}$ were calculated to be 70±10%, 20±10%, and 80±10%, respectively. For the individual sea spray aerosol particles collected on the 0.4-2.8 μm d_a stage,

magnesium was enriched (average 0.40 ± 0.08) relative to seawater (Mg/Na ratio = 0.11) during April 15–16. Calcium was also enriched relative to seawater (Ca/Na ratio = 0.02) in these sea spray aerosol particles, with Ca/Na ratios of 0.06 ± 0.02 during April 1516 and 0.23 ± 0.08 during April 16, as previously observed in Arctic sea salt aerosol (Salter et al., 2016). As discussed above, these divalent cations bind with exopolymeric substances (Krembs et al., 2002) within the sea surface microlayer, resulting in enrichments in organic coatings of the sea spray aerosol (Jayarathne et al., 2016; Bertram et al., 2018; Kirpes et al., 2019).

Submicron sulfate mass concentrations were similar during the low ($U_{9.7m}$ < 4 m s^{-1}) and moderate wind speed periods (averages of 0.7 ± 0.5 μg m^{-3} and 0.7 ± 0.3 μg m^{-3}, respectively; Table S2). Similarly, the majority of supermicron particle sulfate during April 28 – May 4 (66% moderate wind) was also non-sea-salt sulfate ($f_{nssSO_4^{2-}}$ = 76%), further showing the Arctic haze influence. In addition to these observed individual organic+sulfate particles, a fraction of the non-sea-salt sulfate was found to be internally mixed in the individual partially aged sea spray aerosol particles, as previously observed during winter in Utqiaġvik (Kirpes et al., 2018).

For the April 28 – May 4 bulk supermicron particle sample, sodium and chloride concentrations (0.017 μg m^{-3} and 0.014 μg m^{-3}, respectively) were seven and five times, respectively, lower than the average submicron particle sodium and chloride concentrations (0.1±0.2 μg m^{-3} and 0.1±0.1 μg m^{-3}, respectively) during the same period (Fig. 4). The $[Cl^-]/[Na^+]$ ratios were 0.6 mol mol^{-1} and 0.3±0.2 mol mol^{-1} for supermicron and submicron particles, respectively, during this period (April 28 – May 4) (Fig. 5). This further confirms that the supermicron SSA were less chloride-depleted and less aged than submicron SSA during this period (Fig. 5), consistent with the expected shorter atmospheric lifetime, larger chloride reservoir, and smaller surface area to volume ratios for the supermicron aerosols (Leck et al., 2002; Williams et al., 2002; Bondy et al., 2017).

S1.2 Observed and falsely predicted blowing snow periods

Mineral dust, soot, and potassium+sulfur aerosol particles comprised only 0-6%, 0-4%, and 0-2%, by number, respectively,

across the 0.09-0.9 μm d_{pa} range (d_a 0.07-0.4 μm impactor stage) during the observed BLSN period (April 6-7), compared to 0-31%, 0-15%, and 0-6%, by number, respectively, during the moderate wind speed period of April 15-16. Similar to the moderate wind period samples, potassium chloride particles accounted for 47±8%, by number, and mineral dust accounted for 1±1% of the particles collected on the 0.4-2.8 μm d_a impactor stage during April 6 07:00–19:00.

Submicron particle [Ca^{2+}], [Mg^{2+}], and [K^+] also increased during observed BLSN periods (Fig. 4). The submicron particle $f_{nssCa^{2+}}$, $f_{nssMg^{2+}}$, and f_{nssK^+} were 44±11%, 1±4%, and 50±9%, respectively, during observed BLSN periods, suggesting that nearly all of the observed Mg^{2+} and approximately half of the Ca^{2+} and K^+ were associated with sea salt aerosol. The remaining contributions are attributed to the mineral dust and potassium+sulfur particles. Supermicron particle [Ca^{2+}], [Mg^{2+}] and [K^+] were highest during April 7-13 (BLSN winds), lowest during April 28 – May 4 (NBLSN winds), and in between during April 14-20 and April 21-27, which experienced a range of wind speeds (Fig. 4).

The increased [Na^+], [Cl^-], and [Cl^-]/[Na^+] during BLSN wind periods, compared to NBLSN wind periods, were also observed for supermicron particles (Figures 4 and 5). The April 7-13 supermicron particle sampling period covered BLSN wind periods (average $U_{9.7m}$ = 11±2 m s^{-1}; 65% observed BLSN, 35% falsely predicted BLSN). An additional two supermicron samples covered a wide range of wind speeds: April 14-20 ($U_{9.7m}$ = 4-13 m s^{-1}, average 7 m s^{-1}, 9% observed BLSN, 29% falsely predicted BLSN, 58% moderate wind, 4% low wind) and April 21-27 ($U_{9.7m}$ = 0-13 m s^{-1}, average 6 m s^{-1}, 3% observed BLSN, 23% falsely predicted BLSN, 47% moderate wind, 27% low wind). During April 7-13 (BLSN wind), supermicron particle [Na^+] (0.619 μg m^{-3}) and [Cl^-] (0.870 μg m^{-3}) were 35 and 61 times higher, respectively, than during April 28 – May 4 (NBLSN wind, 0.017 μg m^{-3} for [Na^+] and 0.014 μg m^{-3} for [Cl^-]), consistent with a significant supermicron SSA source during April 7-13. The [Na^+], [Cl^-], and [Cl^-]/[Na^+] were also elevated for the submicron particle samples during April 7-13, compared to April 28 – May 4 (Figures 4 and 5). In comparison, the supermicron particle [Na^+] and [Cl^-] during April 14-20 and April 21-27, which covered both BLSN and NBLSN wind periods, were in between the April 7-13 (BLSN wind) and April 28 – May 4 (NBSLN wind) periods (Fig. 4).

For the April 7-13 supermicron particle sample during observed BLSN, the $[SO_4^{2-}]/[Na^+]$ molar ratio was 0.017, which is lower than that of seawater (0.06 mol mol^{-1}; Millero et al., 2008) (Fig. 5). Taken alone, this would be suggestive of a sulfur-depleted supermicron SSA source. However, the average S/Na molar ratio of the 0.4-2.8 μm d_a individual sea spray aerosol particles during the observed BLSN period on April 6 was 0.04 ± 0.01, similar to the ratio of 0.03 ± 0.01 observed during the moderate wind speed period on April 15-16 (Table 3). This suggests that the bulk ratio is an underestimate when considering the distribution of sulfate and sodium across the atmospheric particle population. In comparison, the $[SO_4^{2-}]/[Na^+]$ molar ratios were 0.056 and 0.057, respectively, for the April 14-20 and April 21-27 supermicron particle samples that experienced both BLSN and NBLSN wind speeds (Fig. 5). Therefore, the low bulk $[SO_4^{2-}]/[Na^+]$ ratio for the April 7-13 supermicron particle sample can be explained by the increased $[Na^+]$, from sea spray aerosol generation, at the higher wind speeds, with similar $[SO_4^{2-}]$, from haze aerosol, across the entire wind speed range (Fig. 4).

The bulk submicron particle mass during observed BLSN periods was enriched in sulfate compared to seawater (Fig. 5), and 90±5% of the sulfate was calculated to correspond to secondary non-sea-salt sulfate associated with Arctic haze (Section 3.3.3). This is consistent with the high number fraction of individual aged (Cl depleted, S enriched) sea spray aerosol (0.07-0.4 μm d_a) (Fig. 6), leading to average S/Na ratios of 1.6±0.1 and 2.6±0.2 during observed BLSN (Table 3). In contrast, the bulk supermicron particle $[SO_4^{2-}]/[Na^+]$ during observed BLSN (April 7-13) was 0.017 mol mol^{-1}, which is lower than that of seawater (0.06; Millero et al., 2008) and most similar to that of frost flowers (0.016±0.003; Douglas et al., 2012) (Fig. 5). Yet, frost flowers themselves are not expected to produce aerosols (Domine et al., 2005; Alvarez-Aviles et al., 2008; Roscoe et al., 2011; Yang et al., 2017). However, the average S/Na ratio of the 0.4-2.8 μm d_a individual sea spray aerosol particles during the observed BLSN period on April 6 was 0.04 ± 0.01, similar to the ratio of 0.03 ± 0.01 observed during the moderate wind speed period on April 15-16 (Table 3). This shows that the bulk supermicron $[SO_4^{2-}]/[Na^+]$ ratio is not representative of the individual sea spray aerosol particles.

S1.3 Sea salt aerosol sources during observed blowing snow

The bulk submicron particle mass during observed BLSN periods was enriched in sulfate compared to seawater (Fig. 5), and

90±5% of the sulfate was calculated to correspond to secondary non-sea-salt sulfate associated with Arctic haze (Section 3.3.3). This is consistent with the high number fraction of aged (Cl depleted, S enriched) sea spray aerosol (0.07-0.4 μm d_a) (Fig. 6), leading to average S/Na ratios of 1.6±0.1 and 2.6±0.2 during observed BLSN (Table 3). In contrast, the bulk supermicron particle $[SO_4^{2-}]/[Na^+]$ during observed BLSN (April 7-13) was 0.017 mol mol^{-1}, which is lower than that of seawater (0.06; Millero et al., 2008) and most similar to that of frost flowers (0.016±0.003; Douglas et al., 2012) (Fig. 5). Yet, frost flowers themselves are not expected to produce aerosols (Domine et al., 2005; Alvarez-Aviles et al., 2008; Roscoe et al., 2011; Yang et al., 2017). However, the average S/Na ratio of the 0.4-2.8 μm d_a individual sea spray aerosol particles during the observed BLSN period on April 6 was 0.04 ± 0.01, similar to the ratio of 0.03 ± 0.01 observed during the moderate wind speed period on April 15-16 (Table 3). This shows that the bulk supermicron $[SO_4^{2-}]/[Na^+]$ ratio is not representative of the individual sea spray aerosol particles.

The average $[Mg^{2+}]/[Na^+]$ molar ratio of the surface snowpack over Beaufort Sea first-year sea ice (0.1; Krnavek et al., 2012) is similar to that of seawater (0.11; Millero et al., 2008). In comparison, springtime blowing snow collected over Utqiaġvik tundra was previously observed to be enriched in magnesium (0.20±0.05; Jacobi et al., 2012). Submicron particles during observed BLSN and supermicron particles during observed + falsely predicted BLSN (April 7-13) showed magnesium enrichment, with $[Mg^{2+}]/[Na^+]$ of 0.13±0.01 and 0.15, respectively (Fig. 5). The individual 0.07-0.40 μm d_a sea spray aerosol particles collected overnight from April 6 19:00 to April 7 07:00 also showed magnesium enrichment, with an average Mg/Na of 0.17±0.02 mol mol^{-1} (Table 3). The individual 0.4-2.8 μm d_a sea spray aerosol particles, collected during April 6 daytime showed significant magnesium enrichment of 0.34±0.03 (Mg/Na), similar to during the moderate wind conditions (0.40±0.08 and 1.2±0.4) (Table 3). Similar to the observed calcium enrichment, the magnesium enrichment in both the submicron and supermicron particles is likely due to sea spray aerosol organic coatings enriched in divalent cations, as found from bubble bursting (Kirpes et al., 2019; Jayarathne et al., 2016; Orellana and Leck, 2015; Salter et al., 2016). The brine of frost flowers is also enriched in magnesium ($[Mg^{2+}]/[Na^+]$=0.135±0.005 mol mol^{-1}, Douglas et al., 2012; 0.20±0.05, Jacobi et al., 2012), leading as speculated in a previous field study in Greenland by Hara et al. (2017) to speculate that the sublimation of blowing snow influenced by frost flower brine would also be enriched in magnesium, relative to seawater. However, frost

flower brine influence would be expected to also lead to significant sulfate depletion, which was not observed, as discussed below (Table 3, Figure 5, and Table S3), suggesting contribution from bubble bursting sea spray aerosol production is most likely.

The $[Mg^{2+}]/[Na^{+}]$ of the local tundra surface snowpack during observed BLSN periods was 0.07±0.01 mol mol^{-1}, lower than that of seawater (0.11; Millero et al., 2008), the bulk submicron and supermicron aerosol, previous blowing snow observations, and previous first-year sea ice surface snow (Fig. 5), as discussed above. Krnavek et al. (2012) also found magnesium depletion in some of their springtime Utqiaġvik tundra surface snowpack samples. Notably, the individual 0.07-0.4 μm d_a sea spray aerosol particles collected on April 6 also showed magnesium depletion, with an average Mg/Na of 0.06±0.01 (Table 3). Of the seven individual particle sampling periods analyzed, this was the only period with magnesium depleted sea spray aerosol particle present. The reason for this observed magnesium depletion is not known. Conversely, the larger individual sea spray aerosol particles (0.4-2.8 μm d_a) collected during the same time period were enriched in magnesium, as discussed above (Table 3). The similarity between the local tundra surface snowpack and 0.07-0.4 μm d_a sea spray aerosol particle composition is notable. However, it should be noted that the observed individual sea spray aerosol particles were depleted in Cl and enriched in both S and Ca, in contrast to the tundra surface snowpack (Table 3 and Figure 5).

S2. Organic+sulfate particles

It is important to define what we mean by organic aerosol. The key is that the organic aerosol category here does not have any sodium or magnesium present, which aerosol emitted from ocean water (SSA) will have (Ault et al., 2013). In Figure S4 we are referring to organic aerosol as not being internally mixed with Na, Mg, K, and Ca as measured by EDX (Ault et al., 2013). It is thus straightforward to separate aged SSA (containing Na) and organic aerosol (not containing Na) from secondary or transported primary sources, as we have done in prior studies (Bondy et al., 2017; Gunsch et al., 2017; Kirpes et al. 2018). While there are some contributions to the C from the substrate, the high C peak for the organic aerosol is indicative of a particle that is primarily carbon. We have quantified C in SSA in other papers where samples were collected

on silicon wafers (Kirpes et al., 2019).

Table S1. The NH_4^+, NO_3^-, Br^-, MSA^-, and oxalate ($C_2O_4^{2-}$) mass concentrations (average ± 1σ) for daily submicron particle samples during observed BLSN, falsely predicted BLSN, moderate wind, and low wind periods, and for supermicron particles collected on April 7-13, April 14-20, April 21-27, and April 28-May 4. The LODs for the IC analysis are based on the method calibration curve. Sample values [in µg] less than the average blank value [in µg] +2 σ are excluded/marked as below LOD. After correcting for the blank value, the mass measured is divided by the air volume sampled. If any of these falls below the 0.0002 ug/m^3 (Na^+, Cl^-) or 0.0001 ug/m^3 (all others), they are excluded.

Sample type	Category	$[NH_4^+]$ (µg m^{-3})	$[NO_3^-]$ (µg m^{-3})	$[Br^-]$ (ng m^{-3})	$[MSA^-]$ (µg m^{-3})	Oxalate (µg m^{-3})
Submicron particles	Observed BLSN	0.21±0.05	0.03±0.01	1.8±0.8	0.002±0.002	0.009±0.002
	Falsely Predicted BLSN	0.22±0.05	0.021±0.008	2±1	0.003±0.003	0.009±0.003
	Moderate wind	0.23±0.09	0.02±0.01	2±1	0.007±0.006	0.008±0.003
	Low wind	0.2±0.1	0.020±0.009	1.2±0.6	0.008±0.006	0.006±0.002
Supermicron particles	04/7-13	< LOD	0.022	0.3	< LOD	0.0012
	04/14-20	< LOD	0.013	0.1	< LOD	0.0004
	04/21-27	< LOD	0.032	< LOD	0.0002	0.0015
	04/28-05/04	< LOD	0.008	0.1	0.0002	0.0010

[1] https://saga.pmel.noaa.gov/data/stations/PMEL_Chemistry_Station_readme%20061009.txt

Table S2. The Na^+, Cl^-, SO_4^{2-}, Ca^{2+}, Mg^{2+}, and K^+ concentrations (average ± 1σ) for daily submicron particle samples during observed BLSN, falsely predicted BLSN, moderate wind, and low wind periods, and for supermicron particles collected on April 7-13, April 14-20, April 21-27, and April 28-May 4. The submicron particle mass concentrations (average ± 1σ) during the four supermicron particle collection periods are also shown for comparison.

Sample type	Category	$[Na^+]$ ($\mu g\ m^{-3}$)	$[Cl^-]$ ($\mu g\ m^{-3}$)	$[SO_4^{2-}]$ ($\mu g\ m^{-3}$)	$[Ca^{2+}]$ ($\mu g\ m^{-3}$)	$[Mg^{2+}]$ ($\mu g\ m^{-3}$)	$[K^+]$ ($\mu g\ m^{-3}$)
Submicron particles	Observed BLSN	0.5±0.3	0.9±0.7	0.7±0.2	0.03±0.02	0.07±0.04	0.03±0.02
	Falsely Predicted BLSN	0.3±0.1	0.3±0.2	0.7±0.2	0.02±0.01	0.03±0.02	0.02±0.01
	Moderate wind	0.2±0.1	0.1±0.1	0.7±0.3	0.02±0.01	0.02±0.01	0.02±0.01
	Low wind	0.1±0.2	0.1±0.2	0.7±0.5	0.01±0.01	0.02±0.02	0.02±0.01
	04/7-13	0.3±0.2	0.5±0.4	0.6±0.1	0.020±0.009	0.05±0.02	0.02±0.01
	04/14-20	0.1±0.1	0.1±0.1	0.6±0.1	0.014±0.004	0.02±0.01	0.01±0.01
	04/21-27	0.3±0.1	0.3±0.1	1.0±0.3	0.022±0.004	0.04±0.01	0.03±0.01
	04/28-05/04	0.1±0.2	0.1±0.1	0.7±0.5	0.013±0.008	0.02±0.01	0.02±0.01
Supermicron particles	04/7-13	0.619	0.870	0.045	0.030	0.100	0.034
	04/14-20	0.083	0.133	0.019	0.006	0.012	0.004
	04/21-27	0.341	0.570	0.081	0.020	0.036	0.014
	04/28-05/04	0.017	0.014	0.018	0.005	0.004	0.002

Table S3. The $[Cl^-]/[Na^+]$, $[SO_4^{2-}]/[Na^+]$, $[Ca^{2+}][Na^+]$, $[Mg^{2+}]/[Na^+]$, and $[K^+]/[Na^+]$ molar ratios for submicron particles (average ± 1σ) and local tundra surface snowpack (average ± 1σ) for the categories of observed blowing snow (BLSN), falsely predicted BLSN, moderate wind, and low wind speeds. The corresponding data for the four supermicron particle samples is shown, with comparison to the average (± 1σ) for the submicron particle ion ratios during those periods. Comparison is shown to previous measurements of sea ice surface snowpack (Krnavek et al., 2012), blowing snow (Jacobi et al., 2012), frost flowers (Douglas et al., 2012), and seawater (Millero et al., 2008).

Sample type	Category	$[Cl^-]/[Na^+]$ (mol mol^{-1})	$[SO_4^{2-}]/[Na^+]$ (mol mol^{-1})	$[Ca^{2+}]/[Na^+]$ (mol mol^{-1})	$[Mg^{2+}]/[Na^+]$ (mol mol^{-1})	$[K^+]/[Na^+]$ (mol mol^{-1})
Submicron particles[1]	Observed BLSN	0.9±0.3	0.5±0.4	0.04±0.01	0.13±0.01	0.04±0.01
	Falsely predicted BLSN	0.8±0.2	0.8±0.4	0.05±0.02	0.13±0.01	0.05±0.01
	Moderate wind	0.5±0.2	1.4±0.6	0.08±0.03	0.14±0.05	0.09±0.05
	Low wind	0.4±0.2	1.6±0.7	0.08±0.03	0.11±0.05	0.15±0.08
	04/7-13	0.9±0.2	0.5±0.3	0.036±0.004	0.13±0.01	0.04±0.01
	04/14-20	0.6±0.2	1.5±0.6	0.09±0.03	0.18±0.04	0.08±0.03
	04/21-27	0.7±0.1	0.9±0.2	0.05±0.01	0.12±0.01	0.06±0.02
	04/28-05/04	0.3±0.2	1.6±0.6	0.07±0.02	0.14±0.02	0.11±0.06
Supermicron particles[1]	04/7-13	0.9	0.017	0.03	0.15	0.03
	04/14-20	1.0	0.056	0.04	0.14	0.03
	04/21-27	1.1	0.057	0.03	0.10	0.02
	04/28-05/04	0.6	0.261	0.16	0.23	0.08
Tundra surface snowpack[1]	Observed BLSN	1.1±0.1	0.04±0.01	0.033±0.004	0.07±0.01	0.019±0.004
	Falsely predicted BLSN	1.3±0.4	0.05±0.01	0.025±0.007	0.07±0.02	0.019±0.006
	Moderate wind	1.3±0.3	0.3±0.4	0.2±0.2	0.1±0.1	0.05±0.03
	Low wind	1.4±0.4	0.5±0.5	0.2±0.2	0.2±0.1	0.06±0.05
Sea ice surface snowpack[2]		1.2	0.04	0.02	0.10	0.02
Blowing snow[3]		1.21±0.07	0.03±0.01	0.06±0.02	0.20±0.05	0.022±0.003
Frost Flowers[4]		1.32±0.03	0.016±0.003	0.0216±0.0009	0.135±0.005	0.0239±0.0009
Seawater[5]		1.2	0.06	0.02	0.11	0.02

[1] This study [2] Krnavek et al. (2012) [3] Jacobi et al. (2012) [4] Douglas et al. (2012) [5] Millero et al. (2008)

Table S4. The Na^+, K^+, Ca^{2+}, Mg^{2+}, Cl^-, NO_3^-, Br^-, and SO_4^{2-} concentrations (average ± 1σ) for local tundra surface snowpack samples during observed BLSN, falsely predicted BLSN, moderate wind, and low wind periods.

Tundra snowpack	$[Na^+]$ (μM)	$[K^+]$ (μM)	$[Ca^{2+}]$ (μM)	$[Mg^{2+}]$ (μM)	$[Cl^-]$ (μM)	$[NO_3^-]$ (μM)	$[Br^-]$ (μM)	$[SO_4^{2-}]$ (μM)
Observed BLSN	194±57	4±2	6±2	13±6	218±67	4±2	0.2±0.2	8±3
Falsely Predicted BLSN	229±115	5±3	6±4	18±13	280±123	4±2	0.3±0.3	10±5
Moderate wind	151±144	4±3	6±3	14±15	175±168	7±4	0.5±0.3	12±5
Low wind	89±68	2±1	6±1	9±5	105±76	8±4	0.9±0.3	15±5

Table S5. The average (±1σ) particle number concentrations (#/cm^3) for different size bins and wind categories observed during the study.

Particle diameter \ Wind category		Low wind	Moderate wind	Falsely predicted BLSN	Observed BLSN
0.01-0.3 μm d_m	0.01-0.06 μm d_m	13±23	12±12	36±17	56±27
	0.06-0.3 μm d_m	131±88	161±63	193±48	206±37
0.3-10 μm d_o	0.3-1 μm d_o	8±7	12±8	14±4	12±2
	1-4 μm d_o	$(2±3)\times10^{-1}$	$(3±3)\times10^{-1}$	$(14±7)\times10^{-2}$	$(7±3)\times10^{-2}$
	4-5 μm d_o	$(3±3)\times10^{-4}$	$(2±2)\times10^{-4}$	$(1±1)\times10^{-4}$	$(2±2)\times10^{-4}$
	5-10 μm d_o	$(1±1)\times10^{-4}$	$(1±1)\times10^{-4}$	$(1±1)\times10^{-4}$	$(2±3)\times10^{-4}$

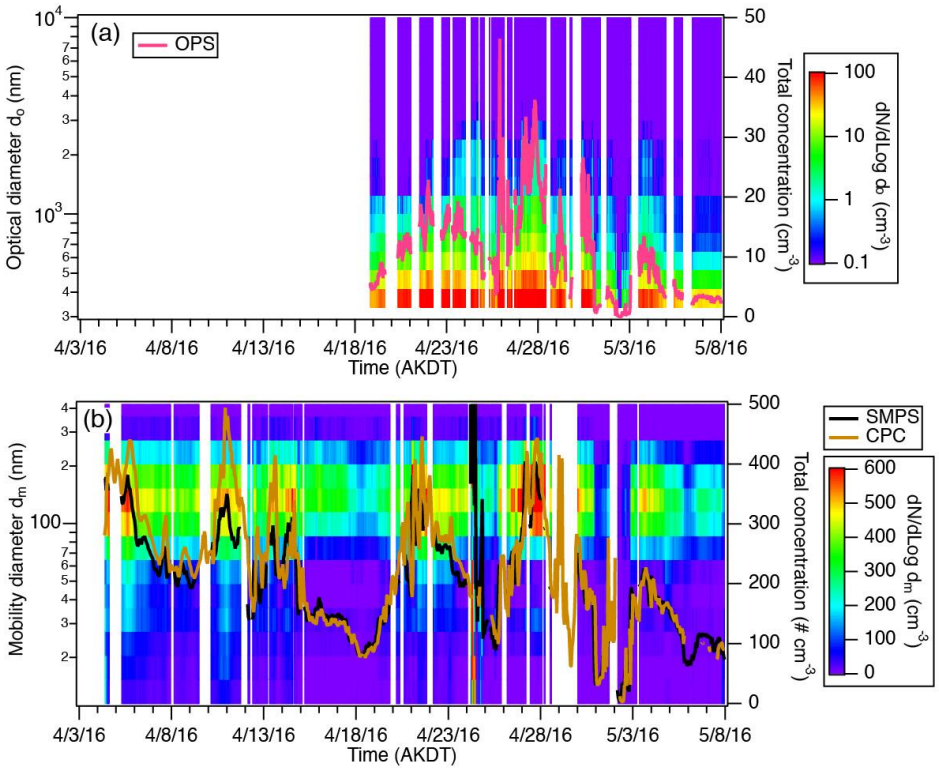

Figure S1. Time series of size distribution of ambient particles measured by (a) an optical particle sizer (OPS) and (b) a scanning mobility particle sizer (SMPS), and total number concentrations measured by the OPS, SMPS, and condensation particle sizer (CPC). Short spikes with total SMPS concentrations > 500 particles cm^{-3} lasting for < 20 minutes were likely local combustion emission and were therefore removed for this data analysis. Spikes in total SMPS concentrations (> 2000 particles cm^{-3}) were observed frequently on April 24 due to nearby generator use, and therefore, this day was also removed for this data analysis.

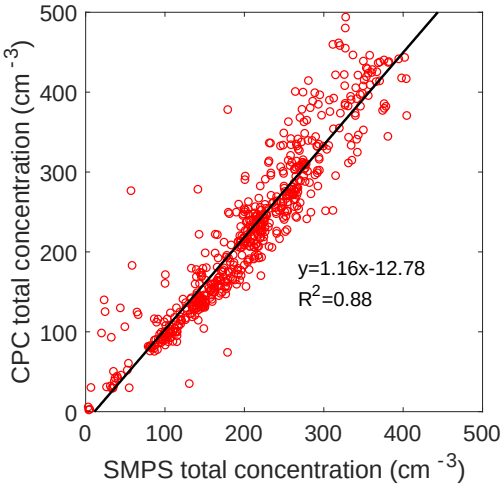

Figure S2. Comparison of hourly average total particle number concentrations measured by SMPS and CPC from April 4 - May 7, 2016.

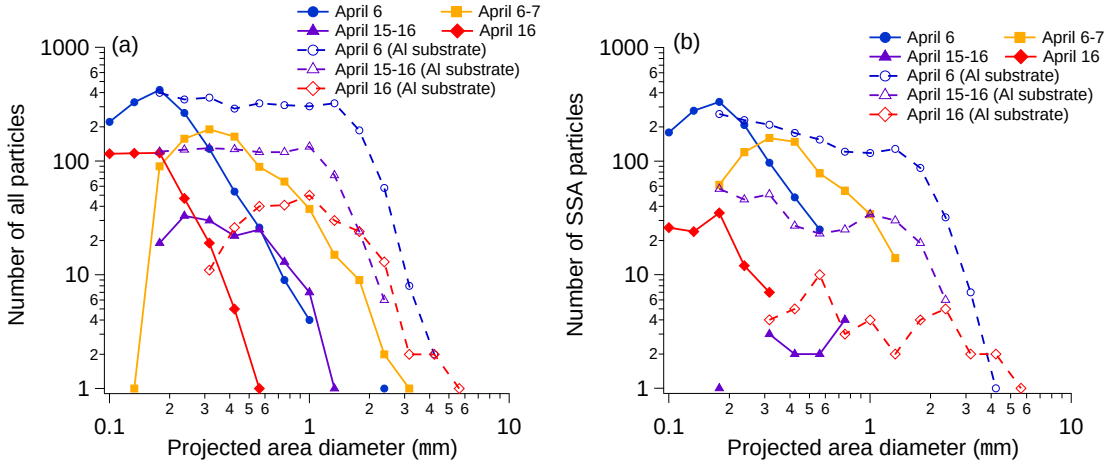

Figure S3. Number of (a) all particles and (b) sea salt aerosol particles identified, using CCSEM-EDX, across the 0.1-6 µm projected area diameter (d_{pa}) range (0.07-2.8 µm d_a impactor stages) for the April 6 07:00-19:00 AKDT, April 6 19:00 – April 7 07:00, April 15 19:00 – April 16 07:00, and April 16 08:00-20:00 samples. As detailed in the methods, 0.07-0.40 µm d_a samples were collected on TEM grids, and 0.4-2.8 µm d_a particles were collected on aluminum (Al) substrate, as noted in legends.

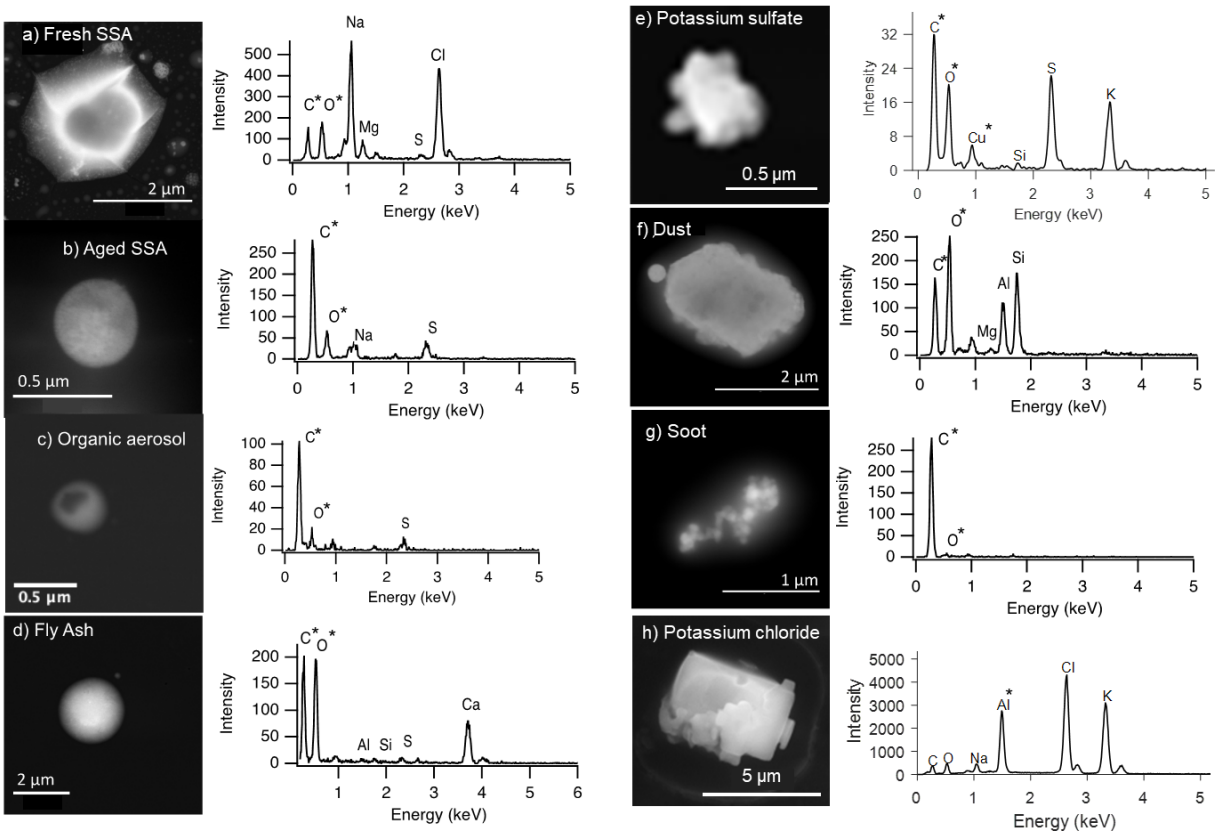

230 **Figure S4.** Representative SEM images and EDX spectra of the main particle types observed in April 6 and April 15-16 samples. The C, O, and Cu signals include contributions from the TEM grids in a-g, and the Al signal includes contributions from the aluminum substrate in h.

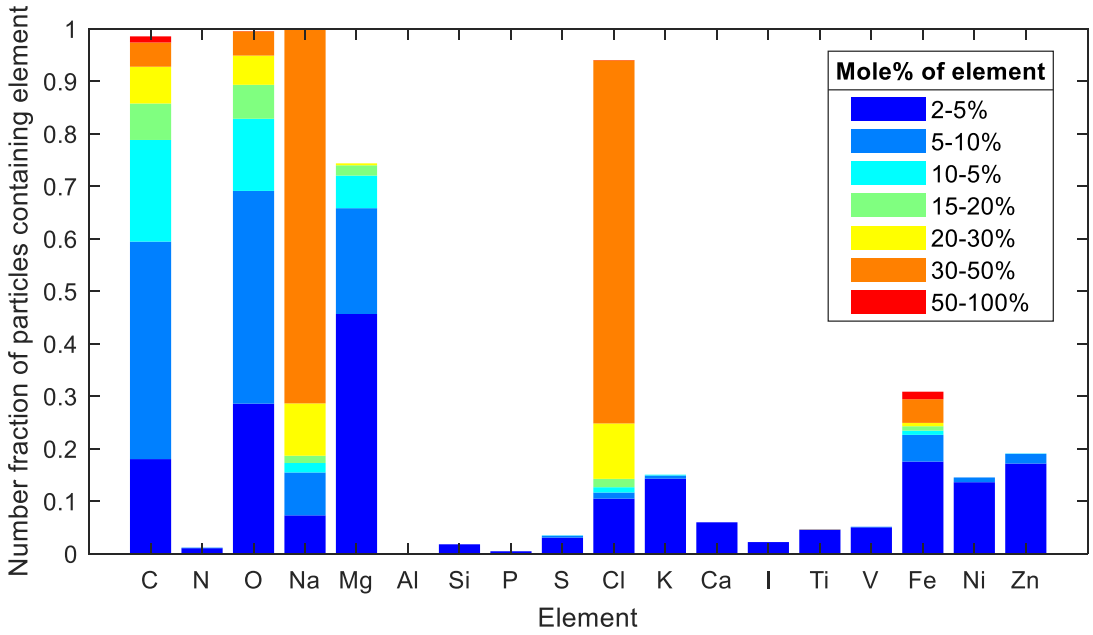

Figure S5. Digital color histogram of individual 0.4-2.8 μm d_a fresh sea spray aerosol particles, collected on aluminum foil. The digital color histogram heights represent the number fractions of individual sea spray aerosol particles containing a specific element, while the colors represent the mole percentage of that element in that number fraction of particles. Aluminum was removed from the EDX spectra due to contributions from the aluminum foil substrate.

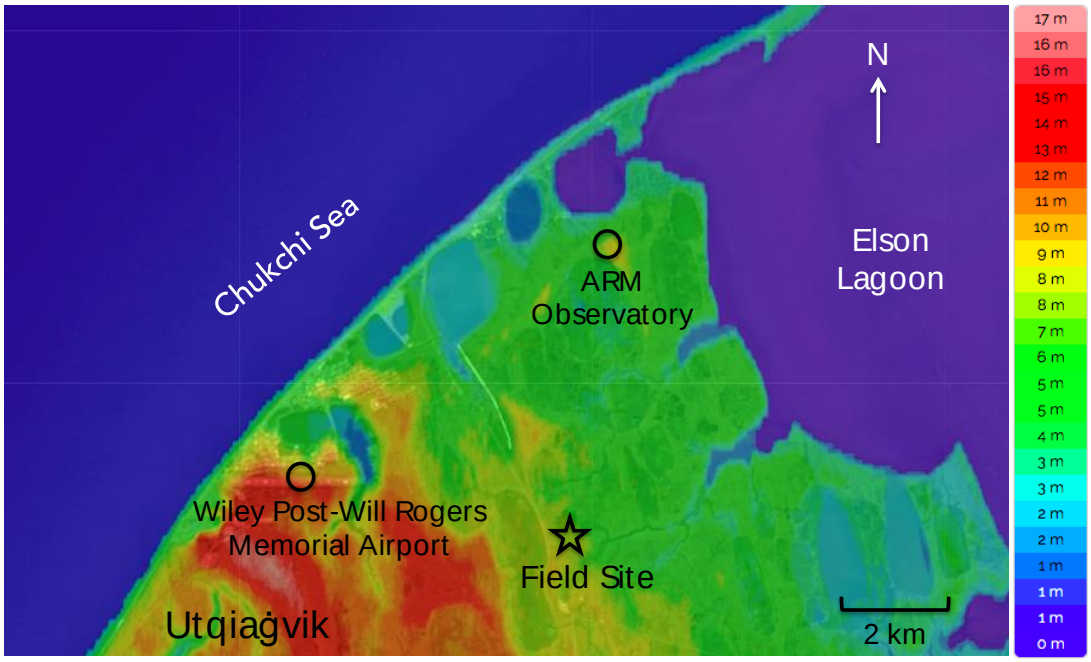

Figure S6. The elevation map of our field site and its surroundings near Utqiaġvik, Alaska. The locations of Field Site, Wiley Post-Will Rogers Memorial Airport, and Department of Energy Atmospheric Radiation Measurement (ARM) Observatory are shown. This map is modified from topographyic-map.com (https://en-ng.topographic-map.com/maps/nqf6/Utqiagvik/).

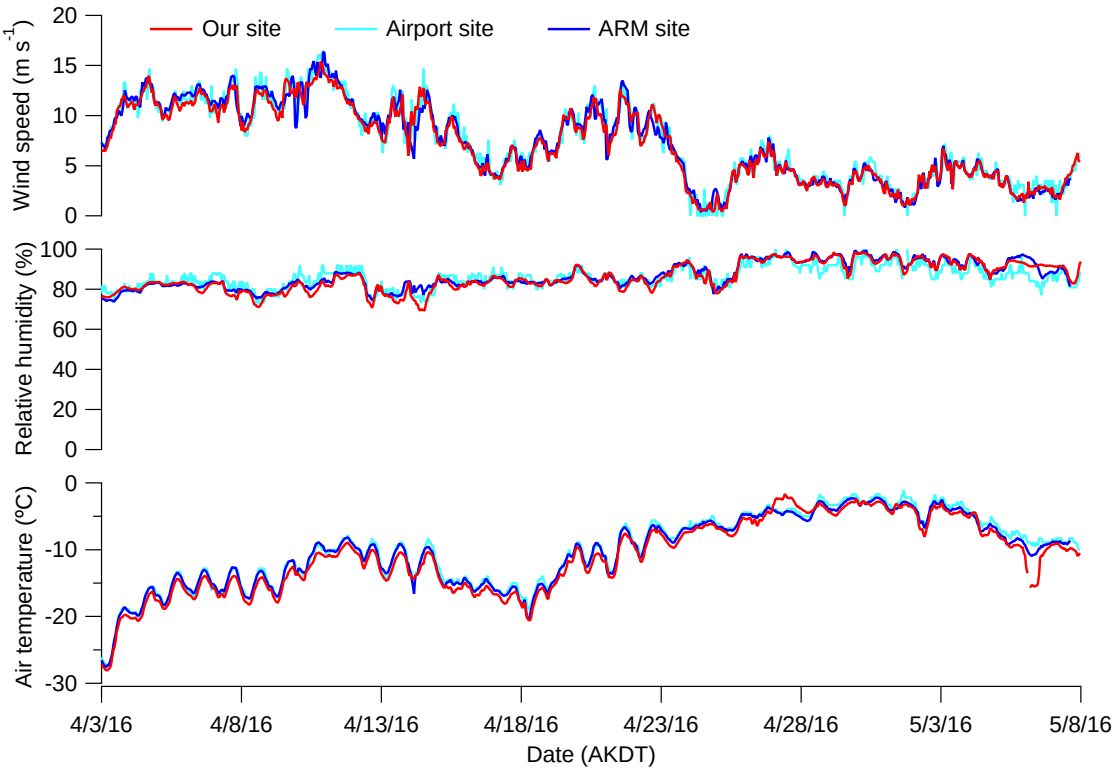

Figure S7. Measured air temperature, relative humidity, and wind speed at Field Site, Wiley Post-Will Rogers Memorial Airport, and Department of Energy Atmospheric Radiation Measurement (ARM) Observatory. The measurement heights at Field site, the airport site, and the ARM site are 10 m, 7 m, and 8 m above the ground, respectively.

Reference

Alvarez-Aviles, L., Simpson, W., Douglas, T., Sturm, M., Perovich, D., and Domine, F.: Frost flower chemical composition during growth and its implications for aerosol production and bromine activation, J. Geophys. Res., 113, D21304, doi:10.1029/2008JD010277, 2008.

Ault, A. P., Moffet, R. C., Baltrusaitis, J., Collins, D. B., Ruppel, M. J., Cuadra-Rodriguez, L. A., Zhao, D. F., Guasco, T. L., Ebben, C. J., Geiger, F. M., Bertram, T. H., Prather, K. A., and Grassian, V. H.: Size-Dependent Changes in Sea Spray Aerosol Composition and Properties with Different Seawater Conditions, Environ. Sci. Technol., 47, 5603–5612, doi:10.1021/Es400416g, 2013.

Bertram, T. H., Cochran, R. E., Grassian, V. H., and Stone, E. A.: Sea spray aerosol chemical composition: elemental and molecular mimics for laboratory studies of heterogeneous and multiphase reactions, Chem. Soc. Rev., 47, 2374-2400, doi: 10.1039/c7cs00008a, 2018.

Bondy, A. L., Wang, B., Laskin, A., Craig, R. L., Nhliziyo, M. V., Bertman, S. B., Pratt, K. A., Shepson, P. B., and Ault, A. P.: Inland Sea Spray Aerosol Transport and Incomplete Chloride Depletion: Varying Degrees of Reactive Processing Observed during SOAS, Environ. Sci. Technol., 51, 9533–9542, doi:10.1021/acs.est.7b02085, 2017.

Domine, F., Taillandier, A. S., Simpson, W. R., and Severin, K.: Specific surface area, density and microstructure of frost flowers, Geophys. Res. Lett., 32, L13502, doi:10.1029/2005GL023245, 2005.

Doorschot, J. J. J. and Lehning, M.: Equilibrium saltation: mass fluxes, aerodynamic entrainment, and dependence on grain properties, Bound.-Lay. Meteorol., 104, 111–130, doi:10.1023/A:1015516420286, 2002.

Douglas, T. A., Domine, F., Barret, M., Anastasio, C., Beine, H. J., Bottenheim, J., Grannas, A. M., Houdier, S., Netcheva, S., Rowland, G., Staebler, R., and Steffen, A.: Frost flowers growing in the Arctic ocean-atmosphere-sea ice-snow interface: 1. Chemical composition, J. Geophys. Res., 117, D00R09, doi:10.1029/2011JD016469, 2012.

Gunsch, M., Kirpes, R., Kolesar, K., Barrett, T., China, S., Sheesley, R., Laskin, A., Wiedensohler, A., Tuch, T., Pratt, K.: Contributions of Transported Prudhoe Bay Oilfield Emissions to the Aerosol Population in Utqiaġvik, Alaska, Atmos. Chem. Phys.**,** 17, 1-29, doi:10.5194/acp-17-10879-2017, 2017.

Hara, K., Matoba, S., Hirabayashi, M., and Yamasaki, T.: Frost flowers and sea-salt aerosols over seasonal sea-ice areas in northwestern Greenland during winter–spring, Atmos. Chem. Phys., 17, 8577–8598, doi:10.5194/acp-17-8577-2017, 2017.

Jacobi, H. W., Voisin, D., Jaffrezo, J. L., Cozic, J., and Douglas, T. A.: Chemical composition of the snowpack during the OASIS spring campaign 2009 at Barrow, Alaska, J. Geophys. Res., 117, D00R13, doi:10.1029/2011jd016654, 2012.

Jayarathne, T., Sultana, C. M., Lee, C., Malfatti, F., Cox, J. L., Pendergraft, M. A., Moore, K. A., Azam, F., Tivanski, A. V., Cappa, C. D., Bertram, T. H., Grassian, V. H., Prather K. A., and Stone, E. A.: Enrichment of saccharides and divalent cations in sea spray aerosol during two phytoplankton blooms, Environ. Sci. Technol., 50, 11511–11520, doi: 10.1021/acs.est.6b02988, 2016.

Krembs, C., Eicken, H., Junge, K., and Deming, J. W.: High concentrations of exopolymeric substances in Arctic winter sea ice: implications for the polar ocean carbon cycle and cryoprotection of diatoms, Deep-Sea Res. Part I Oceanogr. Res. Pap., 49 (12), 2163-2181, doi: 10.1016/S0967-0637(02)00122-X, 2002.

Krnavek, L., Simpson, W. R., Carlson, D., Dominé, F., Douglas, T. A., and Sturm, M.: The chemical composition of surface snow in the Arctic: examining marine, terrestrial, and atmospheric influence, Atmos. Environ., 50, 349–359, doi:10.1016/j.atmosenv.2011.11.033, 2012.

Kirpes, R. M., Bondy, A. L., Bonanno, D., Moffet, R. C., Wang, B., Laskin, A., Ault, A. P., and Pratt, K. A.: Secondary sulfate is internally mixed with sea spray aerosol and organic aerosol in the winter Arctic, Atmos. Chem. Phys., 18, 3937-3949, doi:10.5194/acp-18-3937-2018, 2018.

Kirpes, R. M., Bonanno, D., May, N. W., Fraund, M., Barget, A. J., Moffet, R. C., Ault, A. P., and Pratt, K. A.: Wintertime Arctic sea spray aerosol composition controlled by sea ice lead microbiology, ACS Cent. Sci., 5(11), 1760-1767, doi:10.1021/acscentsci.9b00541, 2019.

Leck, C., Norman, M., Bigg, E. K., and Hillamo, R.: Chemical composition and sources of the high Arctic aerosol relevant for fog and cloud formation, J. Geophys. Res., 107, D12, 4135, doi:10.1029/2001JD001463, 2002.

Millero, F. J., Feistel, R., Wright, D. G., and McDougall, T. J.: The composition of Standard Seawater and the definition of the Reference-Composition Salinity Scale, Deep-Sea Res. Pt. I, 55, 50–72, doi:10.1016/j.dsr.2007.10.001, 2008.

Orellana, M. V. and Leck, C.: Marine Microgels, In Biogeochemistry of Marine Dissolved Organic Matter (Second Edition) (pp. 451–480), Academic Press, doi:10.1016/B978-0-12-405940-5.00009-1, 2015.

Quinn, P. K., Miller, T. L., Bates, T. S., Ogren, J. A., Andrews, E., and Shaw, G. E.: A 3-year record of simultaneously measured aerosol chemical and optical properties at Barrow, Alaska, J. Geophys. Res.-Atmos., 107, AAC 8-1–AAC 8-15, doi:10.1029/2001JD001248, 2002.

Quinn, P. K., Shaw, G., Andrews, E., Dutton, E. G., Ruoho-Airola, T., and Gong, S. L.: Arctic haze: current trends and knowledge gaps, Tellus B, 59, 99–114, doi:10.1111/j.1600- 0889.2006.00238.x, 2007.

Roscoe, H. K., Brooks, B., Jackson, A. V., Smith, M. H., Walker, S. J., Obbard, R. W., and Wolff, E. W.: Frost flowers in the laboratory: Growth, characteristics, aerosol, and the underlying sea ice, J. Geophys. Res., 116, doi:10.1029/2010JD015144, 2011.

Salter, M. E., Hamacher-Barth, E., Leck, C., Werner, J., Johnson, C. M., Riipinen, I., Nilsson, E. D., and Zieger, P.: Calcium enrichment in sea spray aerosol particles, Geophys. Res. Lett., 43, 8277– 8285, doi:10.1002/2016GL070275, 2016.

Williams, J., de Reus, M., Krejci, R., Fischer, H., and Ström, J.: Application of the variability-size relationship to atmospheric aerosol studies: estimating aerosol lifetimes and ages, Atmos. Chem. Phys., 2, 133–145, doi:10.5194/acp-2-133-2002, 2002.

Yang, X., Nedela, V., Runštuk, J., Ondrušková, G., Krausko, J., Vetráková, Ä., and Heger, D.: Evaporating brine from frost flowers with electron microscopy and implications for atmospheric chemistry and sea-salt aerosol formation, Atmos. Chem. Phys., 17, 6291–6303, doi:10.5194/acp-17-6291-2017, 2017.